Semi-annual Report for July - December, 1994
Kendall L. Carder, University of South Florida
~~NASS-31716~~ NAS5-31716

a) Abstract:

The algorithm-development activities at USF continue. Our SeaWiFS chlorophyll a algorithm has been accepted by the SeaWiFS Science Working Group Bio-optical Algorithm subgroup. This is the basis for MODIS pigment algorithm. We continue to refine our version 1 ATBDs(Algorithm Theoretical Basis Document) and β version of algorithms(pigment, IPAR, and clear-water epsilon) for use with MODIS data. These have been submitted to the MODIS Ocean Science team. We also finished two bio-optics cruises, one near the Florida Keys, and one in the Arabian Sea.

b) Task Accomplished:

1. An R/V SUNCOASTER cruise was made from Tampa Bay to the Florida Keys on the Florida shelf between July 26 and 29, 1994. Tasks included partitioning of the absorption coefficients of water samples, taking conductivity, temperature, depth (CTD) data, and chlorophyll fluorescence profiles. We also collected remote sensing reflectance data and samples of bottom sediment for bottom albedo measurements. In-water optical measurements were made using SUDS (Spectral upwelling and downwelling spectrometer).

2. An R/V Thomas Thomson cruise in the Arabian Sea was made from November 28 to December 19, 1994. Tasks included partitioning of the absorption coefficients of water samples, and collecting remote sensing reflectance data. The 32 cruise participants were asembled from the Woods

Hole Oceanography Institute, Naval Research Lab, University of South Florida, University of Oregon, University of Southern California, and Bigelow Labs.

3. Three β version of MODIS products were submitted to the EOS MODIS Project Ocean Science team:

3-1. Determining chlorophyll a concentration and the gelbstoff absorption

coefficient from MODIS water-leaving radiance data.

3-2. Calculating surface PAR(photosynthetically available radiation and IPAR(instantaneous PAR).

3-3. Calculating clear-water epsilons.

The new version of the chlorophyll algorithm is an extension of the irradiance reflectance algorithm for [chl a] discussed in Carder et al. (1991). The major differences between the earlier algorithm and the present one occur in the particle backscattering and phytoplankton absorption terms. Given input $R_{rs}(\lambda)$ values, the algorithm first calculates the absorption coefficient due to phytoplankton at 675 nm, $a_\phi(675)$, and due to gelbstoff at 400 nm $a_g(400)$. Then [chl a] is calculated from the $a_\phi(675)$ value. $a_\phi(\lambda_i)$ for all MODIS wavebands centered at λ_i can then also be calculated from $a_\phi(675)$. The spectral absorption of photons by phytoplanton in the surface layer can later be calculated by combining data from 3-1 and 3-2.

In principle, two spectral ratio equations used to solve for the two unknowns, $a_\phi(675)$ and $a_g(400)$. Based on the spectral shape of the absorption curve for phytoplankton versus those for CDOM and detritus, equations using spectral ratios of 412:443 and 443:555 for $R_{rs}(\lambda)$ provide a good separation of the two types of absorption (see Fig. 1). Signal-to-noise considerations in

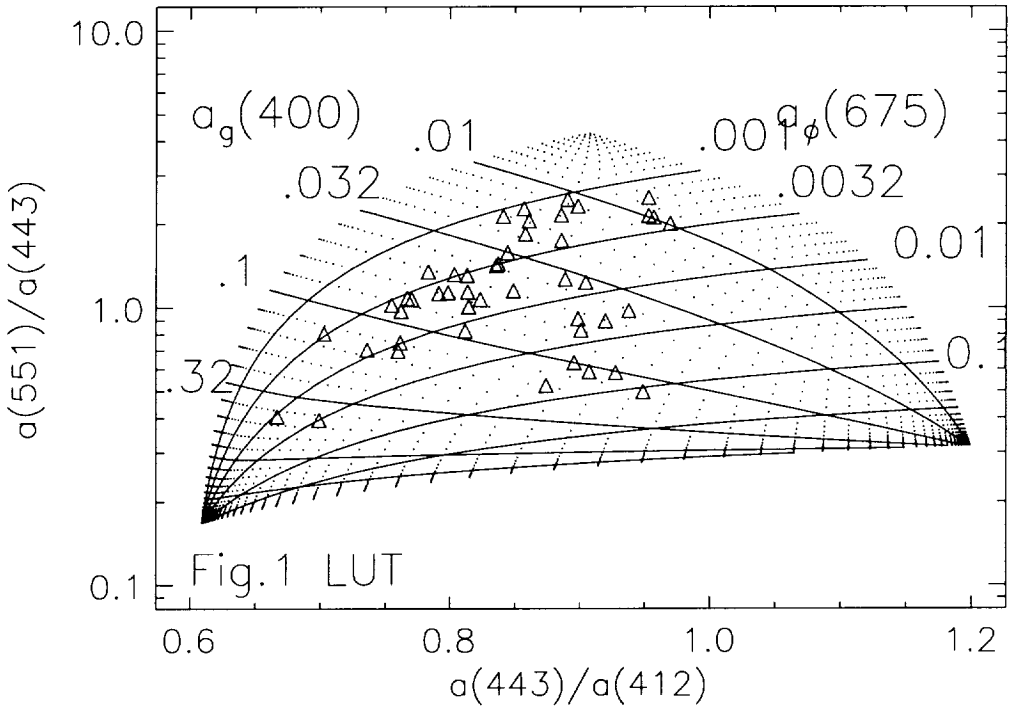

productive waters may make it necessary to switch to other bands (see Fig. 2), but the philosophy behind the algorithm remains the same. Once $a_\phi(675)$ is determined, $a_\phi(\lambda)$ for λ = 412, 443, 490, 510, and 551 nm can be estimated. The equations are solved using lookup tables (LUTs) (see Figures 1, 2). The conversion of $a_\phi(675)$ to [chl a] requires a precise knowledge of the chlorophyll-specific absorption coefficient at 675 nm, a(675). To avoid incomplete extraction

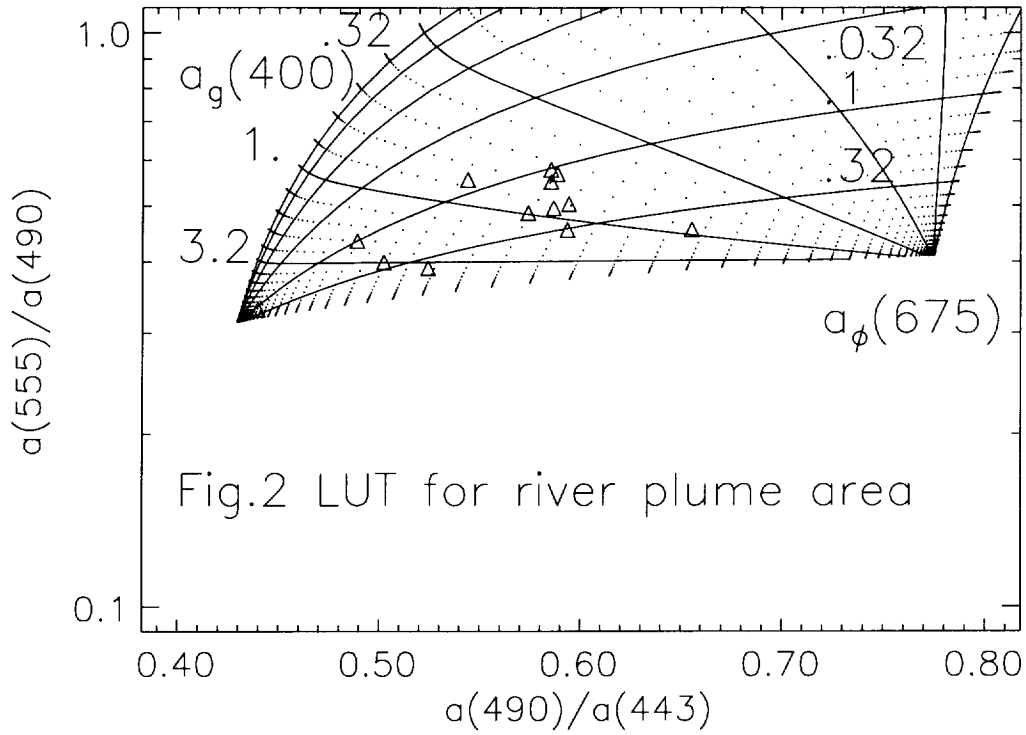

Fig.2 LUT for river plume area

problems, an expression for [chl a] as a function of $a_\phi(675)$ was developed using [chl a] values determined from the pigments extracted from the filter pad on which $a_\phi(\lambda)$ was measured and [chl a] was calculated from the in vitro samples using the methanol specific absorption coefficient of 0.0181 m^2/mg, which is a value determined in our lab on pure chlorophyll a from Sigma Chemicals. Substituting 0.0181[chl a] for $a_{\phi,MeOH}(666)$ in the regression equation results in the following general equation for [chl a] as a function of $a_\phi(675)$

$$[chl \cdot a] = p_0 \left[a_\phi(675) \right]^{p_1}$$

where [chl a] is in mg/m^3 with the coefficients p_0 and p_1 equal to 61.9 and 1.012 for this version of algorithm.

Validation data were separated into two sets of measurements for $R_{rs}(\lambda)$, [chl a], $a_\phi(675)$, and $a_g(400)$ based upon light-hidtory and nutrient availability:

1.) a subtropical data set from the Pacific and Atlantic; and

2.) a low-light, high-nutrient data set. The later consisted of stations from the MLML 1 (cloudy, May, Iceland) and Tambax 2 (cloudy, April, Florida shelf) cruises and of stations above 45° N from the TT010 cruise (cloudy upwelling). Input $R_{rs}(\lambda)$ at the required MODIS wavebands were derived from hyperspectral $R_{rs}(\lambda)$ measurements (see Lee et al., 1994; Lee, 1994) and were weighted to simulate a 10 nm FWHM bandwidth. Measured [chl a], $a_\phi(675)$, and $a_g(400)$ were compared to modeled values (Figs. 3-5), resulting in average rms errors of about 45%. Optimization for subtropical waters is anticipated to improve chlorophyll model accuracy to better than 40% rms error of vhlorophyll-speific absorption function.

It is encouraging that the [chl a] and $a_\phi(675)$ errors are less than 0.5 for subtropical Pacific and Atlantic and high-latitude August data. Also encouraging is the fact that the optical portion of the algorithm performed equally well for data from low-light, high-nutrient aeras. Only one model parameter, p_0, which is related to a(675), needed adjustment to make the [chl a] estimates for the low-light, high-nutrient data as accurate as those for the subtropical data. Nutrient-rich, light- limited conditions produce

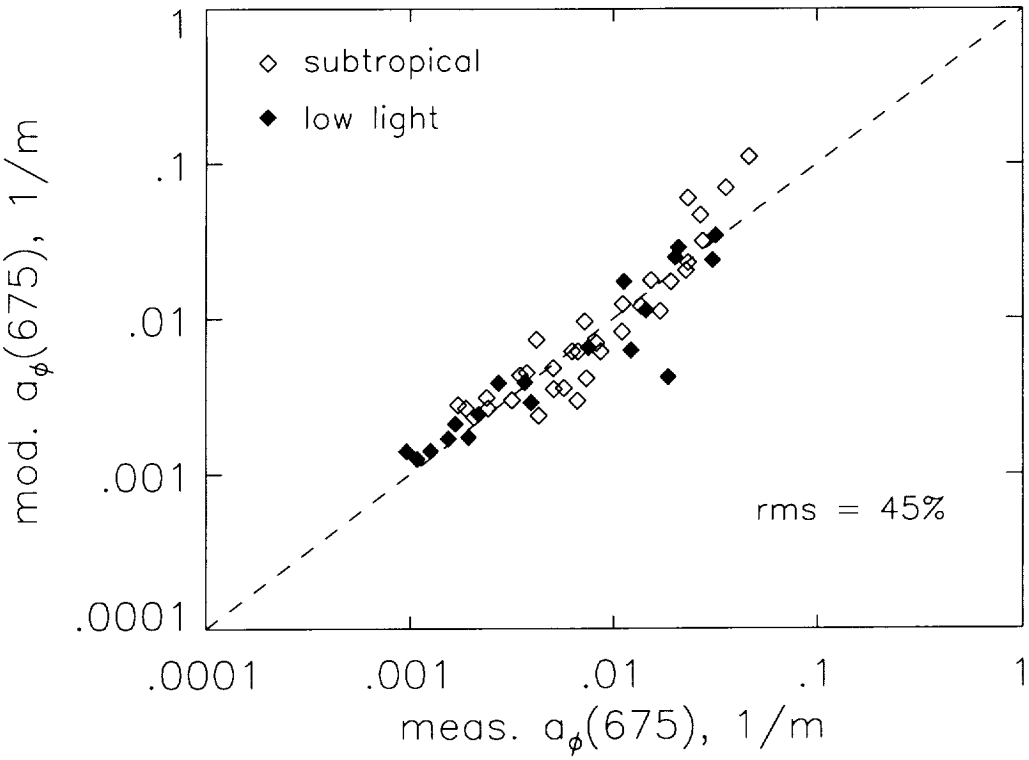
subtropical
low light
rms = 45%
mod. $a_\phi(675)$, 1/m
meas. $a_\phi(675)$, 1/m
1
.1
.01
.001
.0001

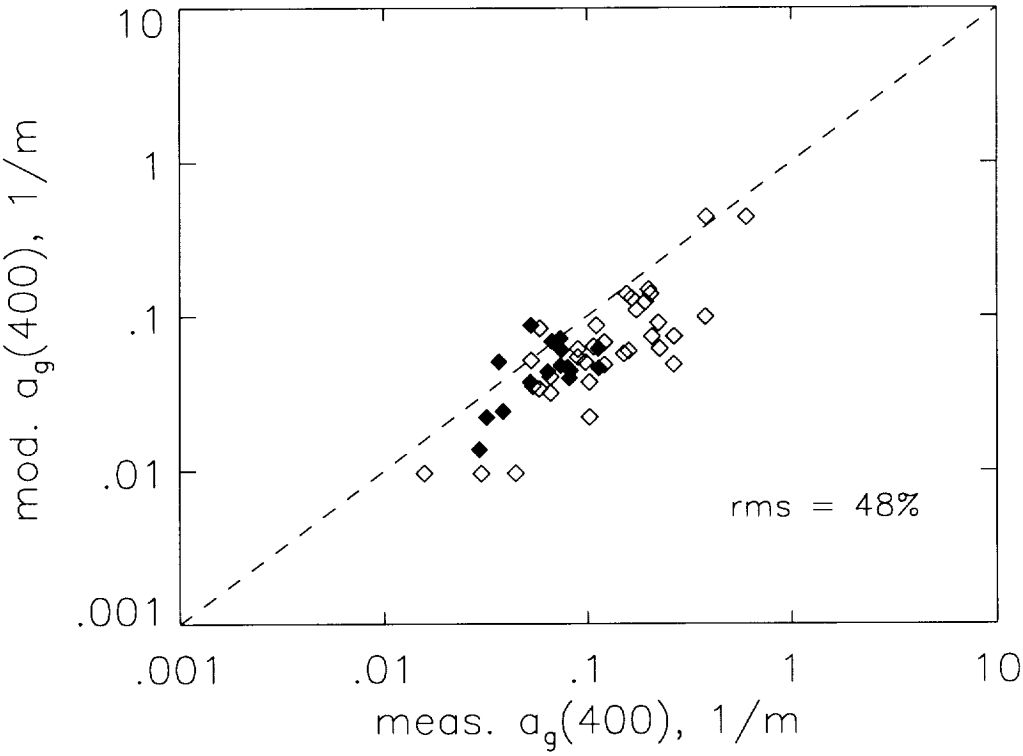
rms = 48%
mod. $a_g(400)$, 1/m
meas. $a_g(400)$, 1/m
10
1
.1
.01
.001

Fig. 8

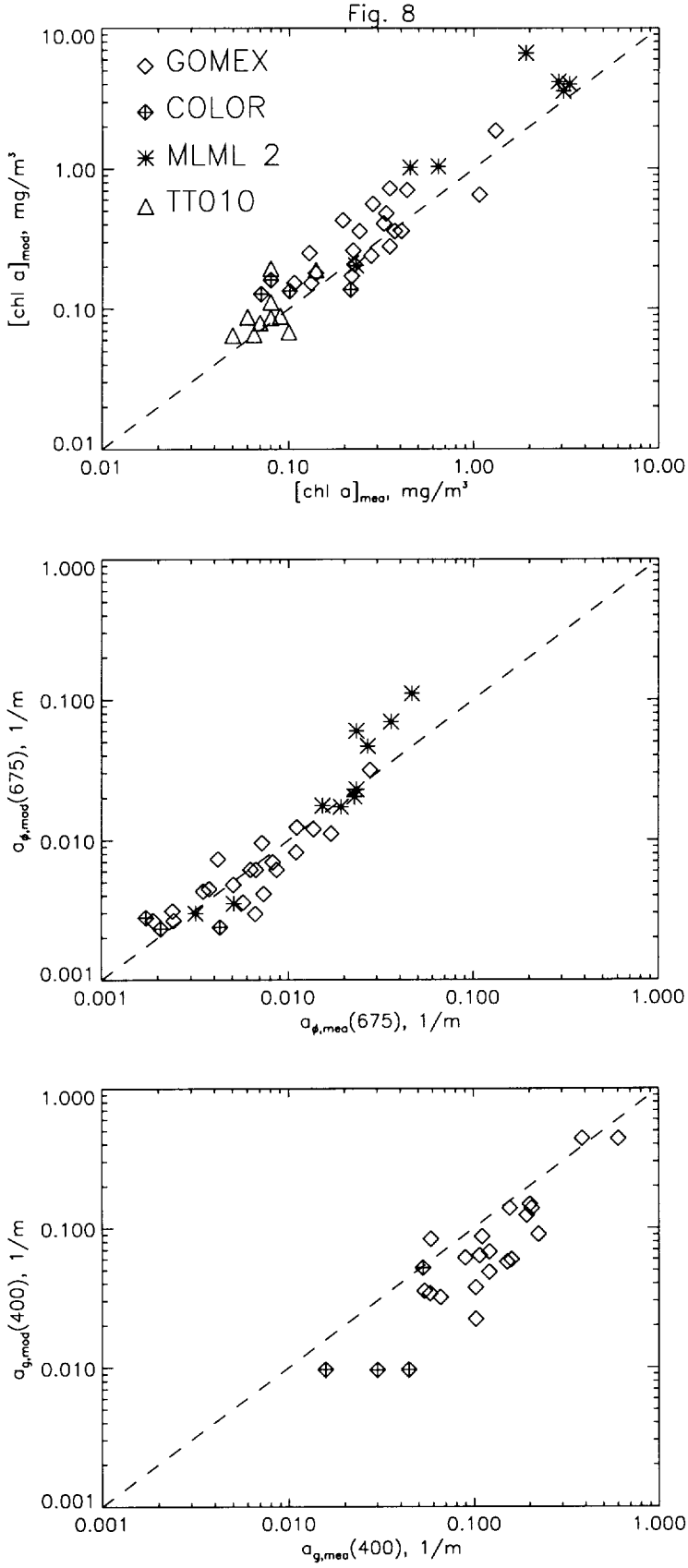
GOMEX
COLOR
MLML 2
TT010
10.00
1.00
0.10
0.01
[chl a]mod, mg/m³
[chl a]mea, mg/m³
1.000
0.100
0.010
0.001
aφ,mod(675), 1/m
aφ,mea(675), 1/m
ag,mod(400), 1/m
ag,mea(400), 1/m

phytoplankton cells that are typically large and pigment-rich, resulting in lower chlorophyll-specific absorption coefficients. These stations were considered to be low-light because of a cloudy light-history prior to measurements.. The parameter p_0 was doubled to reflect the increased pigment packaging expected for low-light-adapted cells, and the [chl a] error was reduced to 0.35. Output values of $a_\phi(675)$ and $a_g(400)$ are not affected by this change.

A major research activity associated with predicting changes in pigment packaging effects is the use of SeaWiFS/AVHRR and OCTS data to identify transition zones between nutrient-limited and nutrient-repleat waters, a reasonable predictor of changes in pigment packaging parameterization.

4. Adjacency Effects: A simple "backward" Monte Carlo technique was used to investigate the effect on the atmospheric point spread function (PSF) (Reinersman and Carder, 1995) of aerosol phase function, sensor viewing angle, aerosol optical thickness, and wavelength. The simulations assumed Lambertian surface reflectance and a stratified, horizontally homogeneous atmosphere in which the scattering and absorbing constituents were distributed according to Elterman's atmospheric profile. It was shown that the magnitude of the near-target PSF depends strongly on the near-forward scattering characteristics and optical thickness of the aerosols between the sensor and target. The near-target asymmetry induced in the PSF by non-nadir viewing is minimal for viewing angles less than 20 degrees but rapidly increases with increased viewing angle. Asymmetric contributions of the far-field at high viewing angles may make it difficult to perform accurate measurement of a dark target lying beyond a bright background. Such a scenario would occur, for instance, if a coastal or estuarine scene were being

observed at a high viewing angle by a sensor with a ground track lying well inland.

An algorithm was devised by which, using the byproducts of the conventional atmospheric correction process to generate the atmospheric PSF, a conventionally processed scene may be corrected for adjacency effect. The correction algorithm is not perfect; it relies on the assumptions that the non-nadir PSF is a scaled version of the nadir PSF, and that the surface beyond the scene is uniform with reflectance equal to the average reflectance of the scene. These assumptions will clearly limit the accuracy of the correction of some scenes, and error in the assumed aerosol phase function may introduce further inaccuracy in the scene correction. But even with these limitations, the correction algorithm has been shown to give reasonable results for a Pine Key, Florida image using AVIRIS data.

Finally, a method of approximating the atmospheric PSF without the Monte Carlo calculations was shown. The simple approximation scheme assumed knowledge of the basic PSFs due to aerosol scattering alone, and due to Rayleigh plus Rayleigh-aerosol interactive scattering. The parameters given for the approximation were based on matching Monte Carlo PSF simulations which used the marine aerosol phase function and an atmospheric aerosol distribution based on Elterman's atmospheric profile. Adjusting the PSF approximation for other conditions would require only two or three Monte Carlo PSF simulations under the chosen conditions. Then the parameters of the approximation scheme could be reset to match the new Monte Carlo results.

Error analysis of the correction algorithm is scene dependent, and has proven to be difficult even with a well-understood data set. However, even

though the error of the correction itself is difficult to quantify, the PSF correction algorithm presented in this paper will point out the relative extent to which pixels of a high-contrast scene are degraded by adjacency effect.

The trend toward higher spatial resolution in satellite and high-altitude spectrometry implies the intent to make accurate measurements in high contrast regions. Atmospheric adjacency effect, however, will induce large fractional errors in measurements of surface-leaving radiance from dark targets in high-contrast settings. Correction for adjacency effect, therefore, will be particularly important for measurement of water-leaving radiance from lakes, rivers, and coastal areas. Adjacency effects more than 2 km from the Pine Key beach were not observed for a very clear atmospheric (visibility > 40 km), suggesting that adjacency effects for MODIS under clear conditions will be less than effects due to stray light and/or electronic overshoots under more turbid atmospheric conditions, however, and for bay waters mostly surrounded by land, correctiond for land-adjacency will be useful.

c) Tasks Anticipated:

Much more field data need to be acquired to better validate the algorithm parameters for varying regions and seasons. In order to derive [chl a], it is vital to predict how $a(\lambda)$ will vary. Thus, we must study the effect on $a(\lambda)$ of 1) light history, which may be related to season, latitude, and recent cloud-cover, and of 2) nutrient history, which is influenced by upwelling, river plumes, and offshore/onshore proximity. We have done extensive field work in the Gulf of Mexico and have developed a general scheme to describe the seasonal variations there: spring bloom, where $a(\lambda)$ is low and detritus is low; summer,

where a(λ) is high and detritus is increasing; and fall, where a(λ) is high and detritus is high. This description should be applicable to other subtropical regions. We have a cruise to the Arabian Sea planned for the summer and just completed the one for fall season, which will provide data sets for a coastal upwelling/high light regime to complement our continuing work in the Gulf of Mexico and our work in the Pacific.

Future versions of the algorithm will include several flags to indicate exceptions such as low $L_W(412)$ and possibly low $L_W(443)$ (i.e., a low signal-to-noise flag), high detritus and/or suspended sediments (indicated by high $L_W(667)$ to $L_W(551)$), bottom reflectance, or cocolithophore blooms. For each flag, provisions can be made for switching to a flag-specific LUT.

d) References cited:

Carder, K. L., S. K. Hawes, K. A. Baker, R. C. Smith, R. G. Steward, and B. G. Mitchell, Reflectance Model for Quantifying Chlorophyll a in the Presence of Productivity Degradation Products, J. Geophys. Res., 96(C11), 20,599-20,611, 1991.

Lee, Z., Visible-infrared Remote-sensing Model and Applications For Ocean Waters, PhD dissertion, USF, Dec. 1994.

Lee, Z., K.L. Carder, S.T. Hawes, R.G. Steward, T.G. Peacock, and C.O. Davis, Model for The Interpretation of Hyperspectral Remote-sensing Reflectance, Applied Optics, Vol. 33(24), Aug. 1994.

Reinersman, P. and K.L. Carder, Monte Carlo Simulation of the Atmospheric Point Spread Function with Application to Correction for Adjacency Effect, Applied Optics, 1995, submitted.